Inertial microfluidics for continuous particle separation in spiral microchannels

Sathyakumar S. Kuntaegowdanahalli,[a] Ali Asgar S. Bhagat,[a] Girish Kumar[b] and Ian Papautsky*[a]

Received 24th April 2009, Accepted 9th July 2009
First published as an Advance Article on the web 21st July 2009
DOI: 10.1039/b908271a

In this work we report on a simple inertial microfluidic device that achieves continuous multi-particle separation using the principle of Dean-coupled inertial migration in spiral microchannels. The dominant inertial forces coupled with the Dean rotational force due to the curvilinear microchannel geometry cause particles to occupy a single equilibrium position near the inner microchannel wall. The position at which particles equilibrate is dependent on the ratio of the inertial lift to Dean drag forces. Using this concept, we demonstrate, for the first time, a spiral lab-on-a-chip (LOC) for size-dependant focusing of particles at distinct equilibrium positions across the microchannel cross-section from a multi-particle mixture. The individual particle streams can be collected with an appropriately designed outlet system. To demonstrate this principle, a 5-loop Archimedean spiral microchannel with a fixed width of 500 μm and a height of 130 μm was used to simultaneously and continuously separate 10 μm, 15 μm, and 20 μm polystyrene particles. The device exhibited 90% separation efficiency. The versatility of the device was demonstrated by separating neuroblastoma and glioma cells with 80% efficiency and high relative viability (>90%). The achieved throughput of ~1 million cells/min is substantially higher than the sorting rates reported by other microscale sorting methods and is comparable to the rates obtained with commercial macroscale flow cytomerty techniques. The simple planar structure and high throughput offered by this passive microfluidic approach make it attractive for LOC devices in biomedical and environmental applications.

1. Introduction

High throughput microparticle separations are becoming indispensable in many lab-on-a-chip (LOC) systems for biomedical[1] and environmental[2] applications. In most LOCs developed for biomedical applications, microparticle separators are used in size-based separation and sorting of cells. For example, efficient separation of human T-lymphocytes (CD4+) from whole blood is a critical step in the diagnosis and treatment of HIV disease.[3] Alternatively, separation of neuroblastoma and glioma cells may have potential applications in cell replacement therapy of neurodegenerative disorders (*e.g.*, Parkinson's disease, Alzheimer's disease, Multiple sclerosis) and cancer.[4,5] Environmental applications of microparticle separators include extraction of harmful bacteria or metal nanoparticles in water quality analysis.[3]

Traditional size-based separation techniques on the macroscale include the use of porous membrane filters. By employing membranes with different pore sizes, multi-component particle filtration can be achieved. However, on the microscale, membrane filtration techniques suffer from various disadvantages including fabrication of complex 3-D structures to define the pore sizes and issues arising from membrane clogging. These factors have limited the popularity of this technique at the microscale leading to the development of numerous membraneless separation techniques.[6]

Electrophoresis[7,8] and dielectrophoresis[9] have been used on the microscale for achieving high resolution particle separation. As the separation principle is size-based, separation of two or more particle sizes can be achieved simultaneously. However, these techniques require an external power source and are unable to process large sample volumes due to batch mode operation. This has resulted in the development of several passive continuous flow separation techniques such as pinched flow fractionation (PFF),[10] sedimentation, hydrodynamic chromatography[11,12] (HDC) and deterministic lateral displacement.[13,14]

Passive separation of two or more particle components simultaneously has been successfully demonstrated on the microscale using PFF[10] and deterministic lateral displacement (DLD)[13,14] based techniques. In PFF, fluid flows with and without particles are introduced into microchannels comprising of a pinched and broadened segment. In the pinched segment, particles are aligned along the channel sidewall by controlling the flow rate of the fluid flow without particles. As the particles travel from the pinched segment to the broadened microchannel segment, smaller particles experience a force directed towards the channel sidewalls while the bigger particles experience a force towards the channel center, thus achieving separation. In deterministic lateral displacement, micro-pillars are suitably placed in the microchannel such that particles larger than the critical diameter $d_c = 20\% \times 2w$ (w is the separation between two pillars) follow a deterministic path leading to the formation of multiple particle streams based on size. The method was successfully used

[a]*Department of Electrical and Computer Engineering, 814 Rhodes Hall, ML030, University of Cincinnati, Cincinnati, OH, 45221, USA. E-mail: ian.papautsky@uc.edu; Fax: (513) 556-7326; Tel: (513) 556-2347*
[b]*Department of Chemical Engineering, University of Cincinnati, Cincinnati, OH, 45221, USA*

to demonstrate efficient sorting of 0.8 μm, 0.9 μm and 1 μm diameter microspheres. Although these techniques operate in continuous mode, the need for narrow channel geometries in PFF and presence of obstructions in DLD may lead to channel clogging and particle–particle interactions. Additionally, the reported throughputs are insufficient for cell sorting and cytometry applications.

Recently, inertial migration based particle filtration techniques have been reported to achieve high throughput particle separation.[15–19] Under the influence of the inertial forces, neutrally buoyant particles flowing in a microchannel migrate to stable equilibrium positions along the channel periphery. Di Carlo *et al.*[18] showed that by employing a curvilinear channel the Dean vortices can be used to reduce the number of equilibrium positions to one. This single particle stream can later be extracted by employing bifurcated outlets. Using this technique rapid microparticle filtration can be achieved.[17–22] For example, we recently demonstrated complete separation of a two particle mixture (7.32 μm and 1.9 μm diameter) by ensuring that the smaller particle motion was affected solely by Dean forces and the larger particle migration by inertial lift forces.[17]

In our previous work,[17] we introduced a design to achieve complete separation of two different particle sizes by exploiting the effects of Dean drag and inertial lift forces. The larger particles equilibrated under the combined influence of the inertial lift forces and the Dean force at the inner microchannel wall. The inertial lift forces however did not affect migration of the smaller particles, which were transposed to the outer microchannel wall due to Dean drag. Since particle separation was not dependent on the ratio of the two forces, a major limitation of the design was its inability to separate more than two particle mixtures irrespective of the number of outlets.

In this paper, we demonstrate for the first time the use of Dean coupled inertial migration to simultaneously separate multi-particle mixtures. In a curvilinear microchannel, a combination of Dean drag and inertial lift forces result in particle equilibration at the inner microchannel wall. The position at which the particles equilibrate is dependent on the ratio of these two forces. In this work we have developed a design which exploits the particle size dependence of the ratio of the two forces to form segregated, focused particle streams which can be extracted by employing a suitable outlet system. Although the design reported herein is similar to the previously reported spiral separators,[17] the working principle for achieving separation is different and is the first demonstration of a multi-particle separation using inertial microfluidics. Additionally, the system reported in this work is simple, easy to fabricate, and is capable of continuously separating particles with a high throughput over a wide dynamic range. The proposed principle was also used to demonstrate size-based cell separation between SH-SY5Y neuroblastoma cells and C6 glioma cells.

2. Design principle

In our recent work,[17] we showed that particles flowing in a spiral microchannel with rectangular cross-section experience a combination of inertial lift and Dean drag forces. The magnitude and direction of these forces depends on the particle size and position across the microchannel cross-section. For particles with $a_p/D_h \geq 0.07$ (where, a_p is particle diameter and D_h is the microchannel hydraulic diameter), the lift forces dominate and are responsible for the particles equilibrating within the microchannel.[17–19] Herein, we demonstrate that the position at which particles of different sizes equilibrate is dependent on the ratio of lift and Dean drag forces which varies with the third power of the particle diameter. By modulating the flow parameters, individual particle streams can be generated for separation applications as shown in Fig. 1.

In a plane Poiseuille flow, the parabolic nature of the velocity profile results in a shear gradient induced inertial lift force that drives the suspended microparticles away from the microchannel center towards the channel walls. As the particles move closer to the channel wall, the rotational wake around the particles is disturbed due to the presence of the wall inducing a lift force on the particles directed away from the wall.[18,23,24] These oppositely directed forces exert a net lift force (F_L) on the particles equilibrating them into focused streams around the microchannel perimeter. Segre and Silberberg were the first to report this effect demonstrating that a uniformly distributed suspension of neutrally buoyant particles form a narrow band at $0.6R$ from the channel center in a circular channel of radius R.[25,26] Chun and

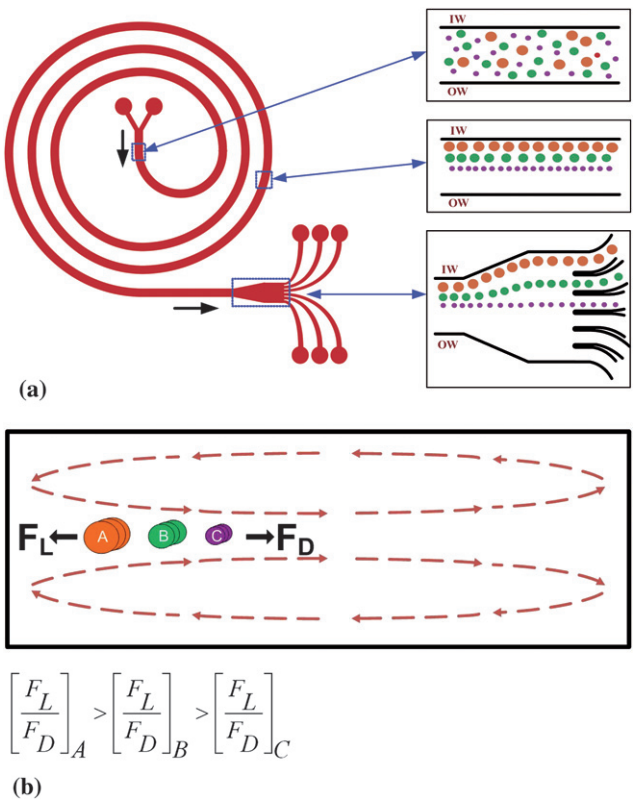

$$\left[\frac{F_L}{F_D}\right]_A > \left[\frac{F_L}{F_D}\right]_B > \left[\frac{F_L}{F_D}\right]_C$$

Fig. 1 (*a*) Schematic of the spiral microparticle separator. The randomly dispersed particles equilibrate at different equilibrium positions along the inner wall (IW) of the spiral microchannel under the influence of F_L and F_D. Separation between individual particle streams is enhanced by opening the spiral channel into a wider straight channel before extracting the individual streams using a multiple outlet design. (*b*) Microchannel cross-section illustrating effects of F_L and F_D on particles. The ratio of forces (F_L/F_D) is the determining factor in where a particle of given size (diameter) equilibrates.

Ladd showed the preferential equilibration of particles with $a_p/D_h \sim 0.1$ in square cross-sectional channels.[27] In our previous work, we showed the equilibrium positions in square and rectangular microchannels at finite Re ($1 < Re < 50$) flows.[15,16]

The net lift force acting on the particle suspended in a plane Poiseuille flow is given by[24]

$$F_L = \rho G^2 C_L a_p^4 \quad (1)$$

where ρ is the density of fluid medium, G is the shear rate of the fluid given by $G = U_{max}/D_h$, U_{max} is the maximum fluid velocity and C_L is the lift co-efficient which is a function of the particle position across the channel cross-section and channel Reynolds number (Re). The magnitude of lift coefficient and hence the lift force rises from zero at the channel center to a maximum value before falling back to zero again at a distance of $\sim 0.2D_h$ away from the channel wall, equilibrating the particles.[24] Beyond this point, the lift coefficient changes sign indicating a dominance of wall-induced lift force.

The curvilinear geometry of a spiral microchannel introduces a centrifugal acceleration component directed radially outward resulting in the formation of two symmetric-counter rotating vortices known as the Dean vortices in the top and bottom halves of the microchannel.[28,29] The magnitude of these Dean vortices can be determined by a dimensionless number known as the Dean Number (De), which is given by

$$De = \frac{\rho U_f D_h}{\mu}\sqrt{\frac{D_h}{2R}} = \mathrm{Re}\sqrt{\frac{D_h}{2R}} \quad (2)$$

For a straight microchannel $De = 0$. Increasing the channel cross-section (D_h) or the flow rate increases De, resulting in stronger Dean forces. A particle suspended in a spiral microchannel experiences a transverse drag force due to these Dean vortices. The expression for the Dean drag force experienced by the particle can be arrived at by assuming Stokes drag.[17,30,31]

$$F_D = 3\pi\mu U_{Dean} a_p = 5.4 \times 10^{-4}\pi\mu De^{1.63} a_p \quad (3)$$

where U_{Dean} is the average Dean velocity given by $U_{Dean} = 1.8 \times 10^{-4} De^{1.63}$.

Particle equilibration in rectangular microchannel cross-section is independent of D_h and rather depends on the shortest channel dimension (microchannel height, H) due to varying shear rates across the channel cross-section.[15,16] Hence, the criterion for particle focusing is $a_p/H \geq 0.07$. We use this result to design low aspect ratio spiral microchannels to enhance the separation between individual particle streams over a wide range of particle sizes. The dependence of ratio of the lift force (F_L) to Dean drag force (F_D) on particle size ($F_L/F_D \propto a_p^3$) and the shear rate modulation in low aspect ratio microchannels have been exploited to demonstrate separation of 10 μm, 15 μm, and 20 μm diameter particles. The dominant inertial lift forces align the randomly distributed particles at the inlet near the inner microchannel wall as the flow progresses downstream. On the other hand, the significant Dean drag force move these focused streams farther away from the channel wall depending on the particle size, with the largest particle being closest to the inner channel wall. This results in the evolution of three distinct particle streams which can be independently extracted by designing appropriate outlets.

3. Experimental methods

The microchannels were fabricated in polydimethylsiloxane (PDMS, Sylgard 184, Dow Corning) using standard soft lithography methods. Briefly, a negative silicon master was fabricated by patterning SU-8 photoresist (2075, Microchem Corp.) of desired height using the conventional photolithography process.[32] Subsequently, PDMS polymer mixed in the ratio of 10:1 with the curing agent was cast onto the fabricated silicon master to form a replica of the device. Following curing on a hotplate for 2 h at 80 °C, the PDMS molds were peeled and input and output ports were cored using a 14 gauge syringe needle. The PDMS mold was then bonded to a 1 mm thick microscopic glass slide to complete the channel using corona wand treatment (BD-20AC, Electro-Technic Products Inc.).

Fluorescently labeled polystyrene particles purchased from Bangs Laboratories were diluted in DI water before testing (~0.05% volume fraction). A syringe pump (KDS101, KD Scientific Inc.) was used to drive syringes filled with the particle solution. To evaluate particle stream positions within the microchannel, high speed images of the microchannel were captured using an inverted epi-fluorescence microscope (IX71, Olympus Inc.) equipped with a 12-bit CCD camera (Retiga EXi, QImaging). Using ImageJ® software, Z-stacked composite images were generated by overlaying a stack of 300 images. The particle stream position was determined by analyzing the gray-scale line scans across the channel width in the composite image.[33]

To demonstrate separation of particle mixtures, a solution containing 10 μm ($\sigma = 0.54$ μm), 15 μm ($\sigma = 0.98$ μm), and 20 μm ($\sigma = 0.5$ μm) diameter polystyrene particles labeled with DAPI, FITC, and TRITC fluorophores respectively was used. The particle streams were viewed and captured separately using appropriate filter cubes. The individual images were superimposed to create a composite image to display the formation of three separate focused particle streams.

To quantify separation efficiency, the outlet streams at each of the eight outlets were collected and analyzed by flow cytometry. The BD LSR II (BD Biosciences) flow cytometer was used to perform the analysis. Individual particle solutions were used as controls to draw the gates on a FSC *vs.* SSC plot. The collected samples were then run through the flow cytometer to determine counts for each of the three particles in all the eight outlets.

To demonstrate cell separations, SH-SY5Y neuroblastoma cells ~15 μm ($\sigma = 5$ μm) in diameter were cultured in Opti-MEM medium containing 10% fetal bovine serum supplemented with L-glutamine. The C6 rat glioma cells ~8 μm ($\sigma = 3$ μm) in diameter were cultured in Ham's F-12 medium containing 15% horse serum and 5% fetal bovine serum supplemented with 0.25 μg/mL amphotericin B, 100 U/mL penicillin, and 100 μg/mL streptomycin. Both cultures were maintained at 37 °C in a humidified atmosphere containing 5% (v/v) CO_2. Cells were cultured in sterile 25 cm^2 flasks (Corning). Cells were sub-cultivated (1:4) three times a week and media was replaced every 48 hours. Sub-confluent monolayers were dissociated with 0.01% trypsin and 5.3 mM EDTA solution, re-suspended in fresh basal

media with 5% serum for further subculture. Cells were never allowed to reach 100% confluent. Prior to testing, the cells were mixed together and diluted in 1× phosphate buffered saline (PBS) solution (0.05% volume fraction). The SH-SY5Y neuroblastoma cells were labeled with CellTracker™ Green (Invitrogen Corp.) for better visualization and to confirm separation. The PDMS based devices were thoroughly flushed with PBS and antibiotics (1 × PSN) before running the cell mixture and all experiments were conducted in a sterile environment.

4. Results and discussion

The fabricated devices consisted of a five loop Archimedean spiral microchannel with two inlets and eight equally spaced outlets (Fig. 2). The spiral designs had an initial radius of curvature of 1 cm, with spacing between the successive spiral loops fixed at 500 μm. Width of microchannels was fixed at 500 μm, while microchannel height was varied from 90 μm to 140 μm. At the outlet, the 500 μm wide channel opened into a 1 mm wide segment to increase spacing between particle streams before splitting into eight 100 μm wide outlets (Fig. 2(*b*)).

In this work, we take advantage of the particle size dependence of the ratio of F_L and F_D in spiral microchannels to separate 10 μm, 15 μm and 20 μm diameter particles. Before testing the particle mixture, particles were tested individually in channels of varying heights and *De*. For each channel height, *De* was increased by increasing the flow rate until a single focused particle stream formed at the outlet. Increasing the flow rate further, resulted in migration of the focused particle stream away from the channel inner wall towards the channel center. As the flow rate increased further, the Dean forces begin to dominate the inertial lift forces resulting in de-focusing of the particle stream. Similar behavior was also noted by Di Carlo *et al.*[18] The equilibrium positions of the particle streams were recorded as a function of *De* and these results were used to select the optimum channel height and flow rate required to demonstrate multi-particle separation.

Fig. 3 shows composite images indicating the position (x) of the 10 μm diameter particle streams as a function of *De* in microchannels of varying height (H = 90 μm–140 μm). The suspension of 10 μm diameter particles was introduced through

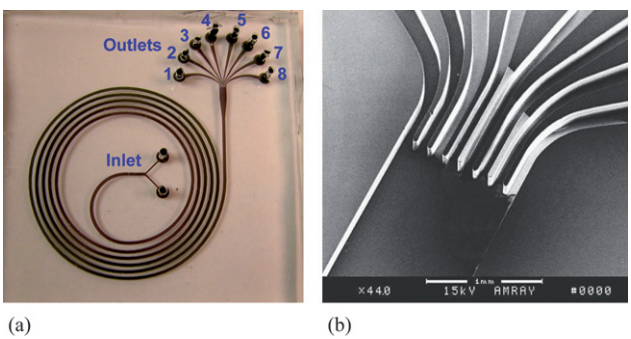

Fig. 2 (*a*) Photograph of the 5-loop spiral microchannel with two inlets and eight outlets fabricated in PDMS (the microchannel is filled with dye for visualization). The outlets are numbered 1–8, starting from the inner channel wall. (*b*) SEM image illustrating the outlet section of the spiral microchannel.

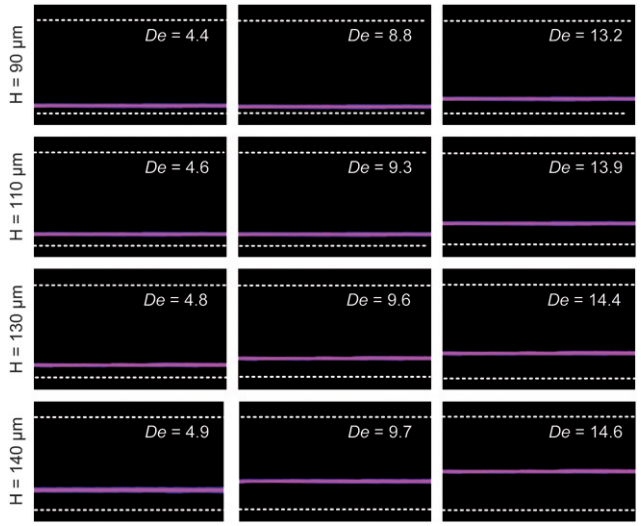

Fig. 3 Fluorescent images (pseudo-colored purple) illustrating the position of the focused 10 μm diameter particle stream in spiral microchannels of different heights at varying *De*.

both inlets and all images were captured in the 500 μm section just prior to the outlet. For a given channel height, the focused particle stream moved away from the channel wall at increasing *De*, indicating the dominance of the Dean force. Although an increase in flow velocity results in a greater lift force ($F_L \propto U_f^2$) as compared to the Dean drag ($F_D \propto U_f^{1.63}$), the stream movement away from the wall can be explained by the decrease in the lift coefficient with increasing fluid flow velocity.[24] Hence, the net lift force reduces with increasing flow velocity and the particle stream moves away from the channel wall. Increasing the channel height also resulted in focusing of particle streams further away from the channel inner wall, which may be explained by the fact that for a given flow velocity U_f the Dean drag force increases with channel height, while the lift force decreases with increasing channel height. Thus, the particle stream position can be altered by either increasing the *De* or increasing the channel height.

Fig. 4(*a*) plots position of particle streams relative to the channel width (W) inside microchannels of different height as a function of *De*. For a 10 μm diameter particle in a 90 μm high channel ($a_p/H \sim 0.11$), the distance of the particle stream from the wall remained constant up to $De = 8.8$ before rising linearly. The lift force acting on the particle below $De = 8.8$ was very much greater than F_D and hence the particle stream was unaffected by an increase in the fluid velocity. However, beyond a critical *De* (flow rate), F_D increases to the same order as F_L and hence the particle stream position varied linearly with the flow rate indicating a dominance of Dean drag. Increasing microchannel height reduced the critical *De* required for particle stream migration, as seen in Fig. 4(*a*), due to a larger Dean force with increase in channel height. Hence, in the case of 130 μm and 140 μm high channels ($a_p/H \sim 0.07$), the particle stream position varied for all flow conditions tested.

For the larger 15 μm diameter particles, the higher a_p/H ratio in the case of the 90 μm and 110 μm microchannels resulted in a larger lift force and hence the particle stream positions remained predominantly constant for increasing *De*. However,

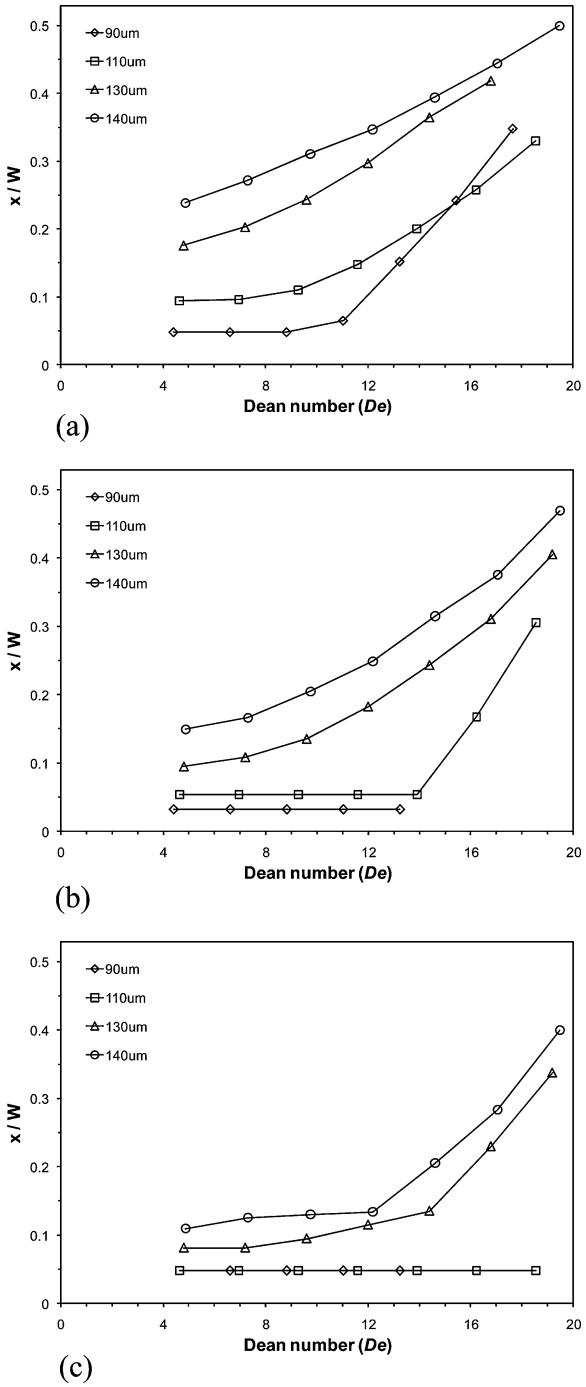

Fig. 4 Plots illustrating position of the (*a*) 10 μm, (*b*) 15 μm, and (*c*) 20 μm diameter particle streams from the inner channel wall for increasing *De* in microchannels ranging from 90 μm to 140 μm in height.

similar to the 10 μm diameter particles, an increase in channel height resulted in a lower $a_p/H \sim 0.1$ ratio and hence the position of the particle stream was strongly influenced by the Dean force. Similarly, the 20 μm diameter particles yielded higher a_p/H, resulting in significant F_L acting on particles in each of the channel heights considered. Hence, a prominent flat (constant position) region is observed in all plots for the 20 μm diameter particles. The increased dominance of the lift force in the case of the larger particles is primarily due to the strong dependence of the lift force on the particle diameter ($F_L \propto a_p^4$ *vs.* $F_D \propto a_p$). Thus, in the 90 μm channel, the 20 μm diameter particle stream position was constant for almost all flows tested.

Results from these individual particle tests indicate that a *complete* separation between the three particle sizes can be achieved in microchannels of different heights and a range of flow conditions. Thus, in the next set of experiments we tested a homogenous mixture of 10 μm, 15 μm, and 20 μm diameter polystyrene particles. Particle separation was experimentally observed by using 10 μm, 15 μm, and 20 μm diameter particles labeled with DAPI, FITC and TRITC fluorophores. Corresponding filter cubes were used to capture images of each of the particle streams at the channel outlet. The captured images were then superimposed to create a composite image showing the three particle streams (Fig. 5). To extract the three individual particle streams, the mixture was tested using the 130 μm high spiral microchannel at $De = 14.4$ (flow rate ~3 mL/min). The 500 μm wide channel opened into a 1 mm wide section prior to the outlet to achieve better separation by taking advantage of the laminar flow profiles in the outlet channels.

The composite images of the inlet and outlet sections are shown in Fig. 5. The image clearly indicates the formation of three distinct particle streams at the microchannel outlet. The position of the 10 μm, 15 μm, and 20 μm particle streams in the 500 μm wide section of the channel were 180 μm, 120 μm, and 65 μm respectively from the inner microchannel wall. Thus, the three particles were collected at the first, second, and third outlets respectively. Although the channel height determines whether the particles focus into a single stream, it is the microchannel width that greatly influences the spacing between individual particle streams. Thus, wider channels result in larger spacing between particle streams, which in turn permits separation of particles with closely spaced diameters. The influence of the microchannel width on the resolving capability of this separation technique is currently being investigated.

The particle streams from each of the eight outlets were collected and analyzed by flow cytometry to quantify the separation efficiency. Fig. 6 presents the cytometry data indicating the particle concentration at the inlet and outlets. Nearly 98% of the particles were filtered out at outlets 1, 2 and 3 (the outlets are numbered starting from the inner wall) suggesting a high degree of particle focusing. Separation efficiency of ~90% was observed between the three particles. Even higher separation efficiencies may be achieved by using mixtures of mono-dispersed particles. Although only separation of three particles sizes has been demonstrated in this work, a larger number of particle sizes can be simultaneously separated by using wider spiral microchannels to increase spacing between the multiple focused particles streams.

Application of the developed technique to high-throughput cell sorting was demonstrated by separation of SH-SY5Y neuroblastoma and C6 glioma cells. Complete separation of these neural stem cells is of critical importance to understanding the specific and unique functions these cells play in the central nervous system (CNS), and potential applications in cell replacement therapy in many neurodegenerative disorders (such as Parkinson's, Alzheimer's, or Multiple sclerosis) and cancer.[4,5]

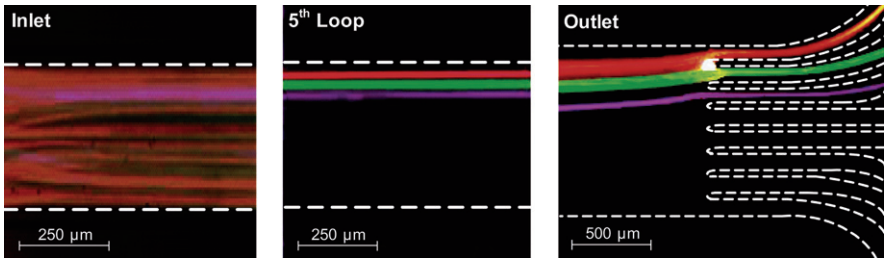

Fig. 5 Superimposed fluorescent images illustrating distribution and position of the 20 μm (pseudo-colored orange), 15 μm (pseudo-colored green), and 10 μm (pseudo-colored purple) diameter particles. The panels represent the inlet, a 500 μm wide channel section just prior to the outlet, and the bifurcated outlet of the 130 μm high spiral microchannel at $De = 14.4$. The randomly distributed particles at the inlet form ordered focused streams which are then collected separately at outlets 1, 2 and 3.

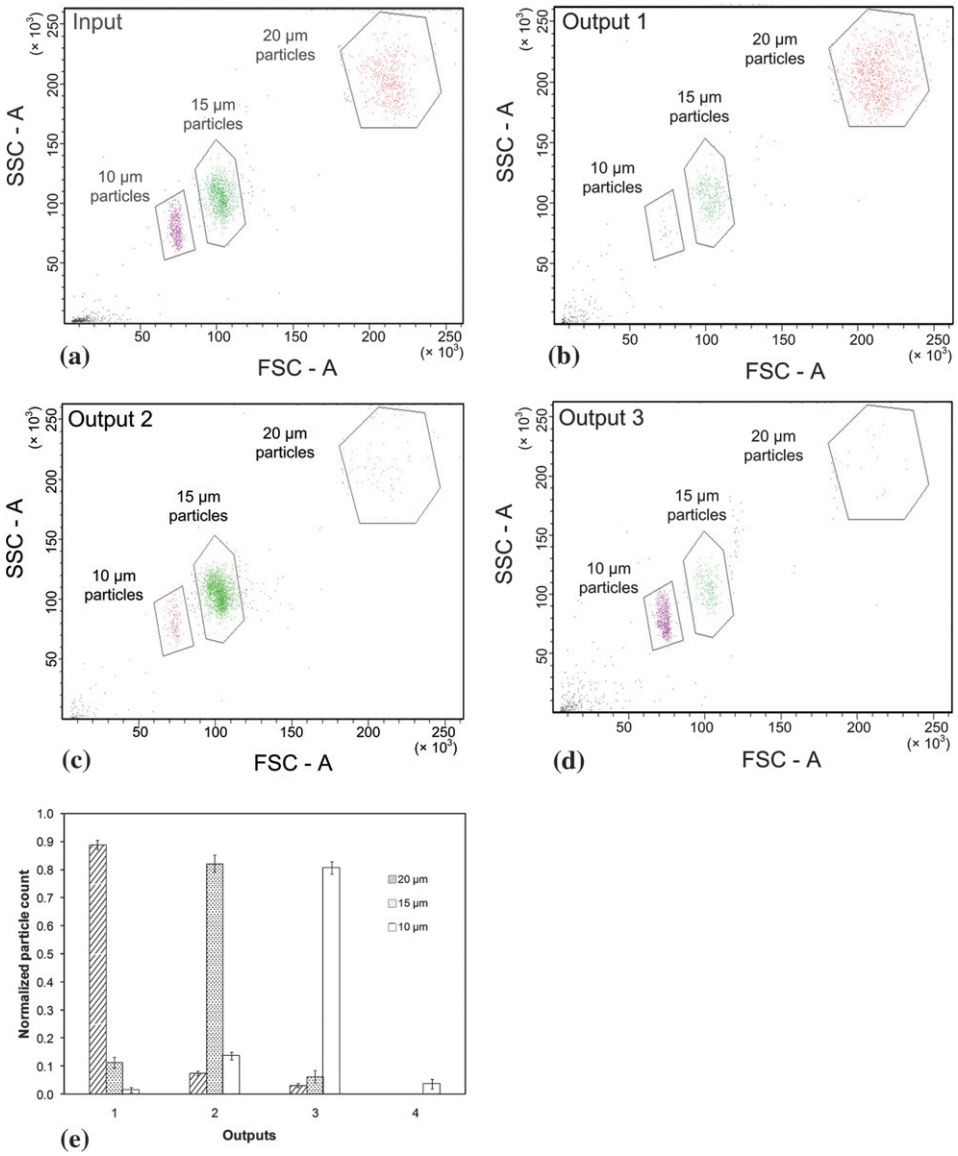

Fig. 6 Flow cytometry data indicating concentration of the three particle mixture. The dot plots indicate concentration of the 10 μm, 15 μm, and 20 μm diameter particles at (*a*) the inlet, and (*b–d*) the first three outlets of the spiral channel. The gates in the side scatter *vs.* forward scatter panels were drawn using pure particle samples in order to discriminate between the three particle sizes. (*e*) Particle counting results illustrating particle distribution across the first four outlets of the spiral microchannel. A ~90% separation efficiency between the three particle sizes was achieved.

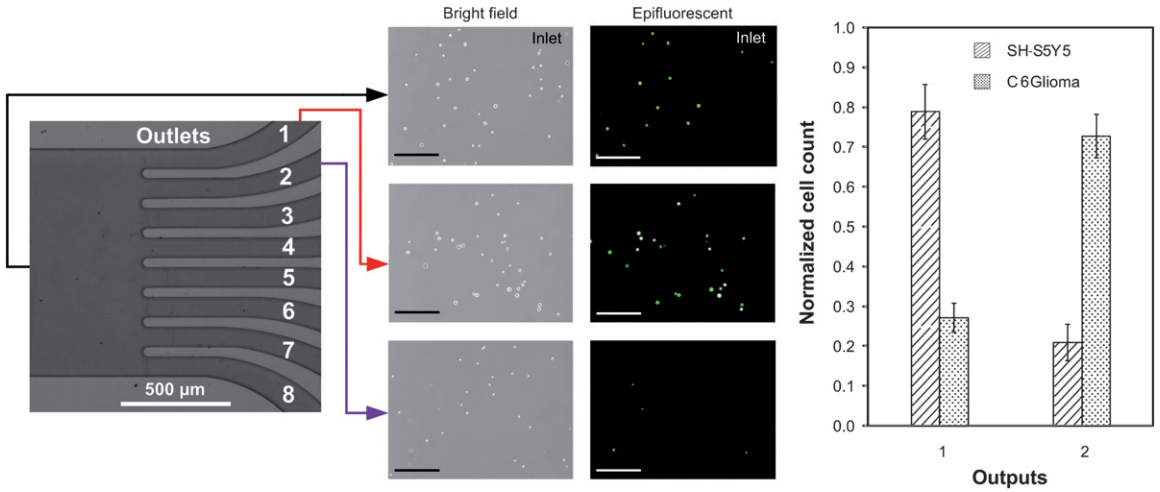

Fig. 7 Bright-field and epifluorescent images illustrating the distribution of the bigger ~15 μm diameter SH-SY5Y cells (pseudo-colored green) and the smaller ~8 μm diameter C6 glioma cells at the inlet and the first two outlets of the spiral microchannel (scale bar 100 μm). Also shown in the figure are the cell counting results clearly indicating ~80% separation efficiency between the two cells types, with the SH-SY5Y cells collected at outlet 1 and the C6 glioma cells at outlet 2.

Based on the size of these cells, the mixture was passed through a 120 μm high microchannel at $De = 11.8$ to collect the bigger ~15 μm diameter cells from outlet 1 and the smaller ~8 μm diameter cells from outlet 2. Fig. 7 shows the bright-field and epifluorescent images illustrating the distribution of the bigger SH-SY5Y cells (fluorescently labeled) and the smaller C6 glioma cells (unlabeled) at the inlet and at the first two outlets of the spiral microchannel. The inlet solution consisted of the two cell mixture with equal cell concentrations (~500,000 × 2 cells/mL). Nearly 90% of the cells were collected at outlets 1 and 2, indicating a high degree of cell focusing. The cell separation efficiency was >80% for both the bigger SH-SY5Y cells at outlet 1 and the smaller C6 glioma cells at outlet 2, but was limited by the large variations in the cell sizes ($\sigma = 5$ μm). A potential concern when separating cells is the possibility of damage to the cells due to the high shear forces. Cell viability following separation was confirmed by bringing both SH-SY5Y neuroblastoma and C6 glioma cells back into culture using the procedure described in the methods section with >90% cell recovery after 24 hrs.

As Pamme[6] discusses in a recent review, continuous flow separation techniques are becoming popular on the microscale due to their ability to achieve high sample throughputs. The average throughput of many of these microfluidic systems is ~2,000 cells/min,[6] although higher throughputs have been recently reported. For example, Fu *et al.*[34] demonstrated a throughput of 1,200–7,200 cells/min while separating *Escherichia coli* cells expressing green fluorescent protein from a background of non-fluorescent *E. coli* cells in microfluidic channels using fluorescently-activated sorting. A similar throughput (~5,400 cells/min) was demonstrated using the PFF approach by Takagi *et al.*[35] who separated erythrocytes from diluted blood.

The developed spiral microparticle separator is ideal for achieving high throughput separations due to the fact that inertial and Dean drag forces acting on particles increase with increasing flow rates. For the flow rates tested (in the mL/min range), a sorting rate of ~1 million cells/min was achieved in our system. This throughput is substantially higher (more than 100×) than the sorting rates achievable by other microscale sorting methods. In fact, the throughput of our system is quite comparable to the sorting rates obtained with commercial flow cytometry techniques, which have a maximum throughput of ~2.4 million cells/min.[36] Since only a 0.05% volume fraction was used in our experiments, the throughput may be increased even further, nearly an order of magnitude, by simply increasing the cell volume fraction and fluid flow rates (volume fraction values of 0.1 to 0.3% have been reported by others[34,35]).

5. Conclusions

In this work, we introduced an inertial microfluidic system for passive simultaneous separation of a microparticle mixture. The effect of Dean coupled inertial migration in spiral microchannels was exploited to generate focused streams of individual particles at distinct positions within the microchannels based on their size. Tests with individual particles were conducted to identify the effects of microchannel height and the Dean number on particle stream position. Based on the results obtained from individual particle experiments, a 130 μm high spiral channel was employed to separate a mixture of 10 μm, 15 μm, and 20 μm diameter particles. The separation efficiency of the device was calculated to be around 90%. The device was also used to show a high throughput (~1 milion cells/min) separation of neural cells with high viability, demonstrating application of this technique in microscale cell sorting. The passive separation principle and the planar nature of the described design will permit easy integration with existing LOC systems requiring high-throughput separations.

Acknowledgements

This work was supported by the University of Cincinnati Institute for Nanoscale Science and Technology and the National Institute of Occupational Safety and Health (NIOSH) Health Pilot Research Project Training Program of the University of Cincinnati Education and Research Center (T42/OH008432-04).

References

1 M. Toner and D. Irimia, *Annu. Rev. Biomed. Eng.*, 2005, **7**, 77–103.
2 G. Blankenstein and U. D. Larsen, *Biosens. Bioelect.*, 1998, **13**, 427–438.
3 M. Kersaudy-Kerhoas, R. Dhariwal and M. P. Y. Desmulliez, *IET Nanobiotechnol.*, 2008, **2**, 1–13.
4 Z. Wu, K. Hjort, G. Wicher and A. Fex Svenningsen, *Biomed. Microdevices*, 2008, **10**, 631–638.
5 E. Hedlund, J. Pruszak, A. Ferree, A. Vinuela, S. Hong, O. Isacson and K. S. Kim, *Stem Cells*, 2007, **25**, 1126–35.
6 N. Pamme, *Lab Chip*, 2007, **7**, 1644–1659.
7 X. Xu, K. K. Caswell, E. Tucker, S. Kabisatpathy, K. L. Brodhacker and W. A. Scrivens, *J. Chromatogr. A*, 2007, **1167**, 35–41.
8 F.-K. Liu, Y.-Y. Lin and C.-H. Wu, *Anal. Chim. Acta*, 2005, **528**, 249–254.
9 M. Durr, J. Kentsch, T. Muller, T. Schnelle and M. Stelzle, *Electrophoresis*, 2003, **24**, 722–731.
10 M. Yamada, M. Nakashima and M. Seki, *Anal. Chem.*, 2004, **76**, 5465–5471.
11 E. Chmela, R. Tijssen, M. T. Blom, H. J. G. E. Gardeniers and A. van den Berg, *Anal. Chem.*, 2002, **74**, 3470–3475.
12 M. T. Blom, E. Chmela, R. E. Oosterbroek, R. Tijssen and A. van den Berg, *Anal. Chem.*, 2003, **75**, 6761–6768.
13 L. R. Huang, E. C. Cox, R. H. Austin and J. C. Sturm, *Science*, 2004, **304**, 987–990.
14 W. Inglis, J. A. Davis, R. H. Austin and J. C. Sturm, *Lab Chip*, 2006, **6**, 655–658.
15 A. A. S. Bhagat, S. S. Kuntaegowdanahalli and I. Papautsky, *Microfluid. Nanofluid.*, DOI: 10.1007/s10404-008-0377-2.
16 A. A. S. Bhagat, S. S. Kuntaegowdanahalli and I. Papautsky, *Phys. Fluids*, 2008, **20**, 101702.
17 A. A. S. Bhagat, S. S. Kuntaegowdanahalli and I. Papautsky, *Lab Chip*, 2008, **8**, 1906–1914.
18 D. Di Carlo, D. Irimia, R. G. Tompkins and M. Toner, *PNAS*, 2007, **104**, 18892–18897.
19 D. Di Carlo, J. F. Edd, D. Irimia, R. G. Tompkins and M. Toner, *Anal. Chem.*, 2008, **80**, 2204–2211.
20 I. Gregoratto, C. J. McNeil and M. W. Reeks, *Proc. SPIE*, 2007, **6465**, 646503.
21 J. Seo, M. H. Lean and A. Kole, *Appl. Phys. Lett.*, 2007, **91**, 033901.
22 J. Seo, M. H. Lean and A. Kole, *J. Chromatogr. A*, 2007, **1162**, 126–131.
23 R. Eichhorn and S. Small, *J. Fluid Mech.*, 1964, **20**, 513–527.
24 E. S. Asmolov, *J. Fluid Mech.*, 1999, **381**, 63–87.
25 G. Segre and A. Silberberg, *J. Fluid Mech.*, 1962, **14**, 136–157.
26 G. Segre and A. Silberberg, *Nature*, 1961, **189**, 209–210.
27 B. Chun and A. J. C. Ladd, *Phys. Fluids*, 2006, **18**, 031704.
28 W. R. Dean, *Phil. Mag. Ser. 7*, 1927, **4**, 208–223.
29 W. R. Dean, *Phil. Mag. Ser. 7*, 1928, **5**, 673–695.
30 S. Ookawara, R. Higashi, D. Street and K. Ogawa, *Chem. Eng. J.*, 2004, **101**, 171–178.
31 S. Ookawara, D. Street and K. Ogawa, *Chem. Eng. Sci.*, 2006, **61**, 3714–3724.
32 A. A. S. Bhagat, E. T. K. Peterson and I. Papautsky, *J. Micromech. Microeng.*, 2007, **17**, 1017–1024.
33 A. A. S. Bhagat and I. Papautsky, *J. Micromech. Microeng.*, 2008, **18**, 085005.
34 A. Y. Fu, C. Spence, A. Scherer, F. H. Arnold and S. R. Quake, *Nature Biotech.*, 1999, **17**, 1109–1111.
35 J. Takagi, M. Yamada, M. Yasuda and M. Seki, *Lab Chip*, 2005, **5**, 778–784.
36 T. D. Chung and H. C. Kim, *Electrophoresis*, 2007, **28**, 4511–4520.

